Journal of Power Sources 196 (2011) 1191–1204

Contents lists available at ScienceDirect

Journal of Power Sources

journal homepage: www.elsevier.com/locate/jpowsour

Exergy analysis of a passive direct methanol fuel cell

Hafez Bahrami, Amir Faghri*

Department of Mechanical Engineering, University of Connecticut, Storrs, CT 06269, USA

ARTICLE INFO

Article history:
Received 24 June 2010
Received in revised form 26 August 2010
Accepted 27 August 2010
Available online 8 October 2010

Keywords:
Direct methanol fuel cell
Exergy
Passive
Irreversibility
Efficiency

ABSTRACT

An analytical, one-dimensional, steady state model is employed to solve for overpotentials at the catalyst layers along with the liquid water and methanol distributions at the anode, and oxygen transport at the cathode. An iterative method is utilized to calculate the cell temperature at each cell current density. A comprehensive exergy analysis considering all possible species inside the cell during normal operation is presented. The contributions of different types of irreversibilities including overpotentials at the anode and cathode, methanol crossover, contact resistance, and proton conductivity of the membrane are investigated. Of all losses, overpotentials in conjunction with the methanol crossover are considered as the major exergy destruction sources inside the cell during the normal operation. While the exergy losses due to electrochemical reactions are more significant at higher current densities, exergy destruction by methanol crossover at the cathode plays more important role at lower currents. It is also found that the first-law efficiency of a passive direct methanol fuel cell increases as the methanol solution in the tank increases in concentration from 1 M to 3 M. However, this is not the case with the second-law efficiency which is always decreasing as the concentration of the methanol solution in the tank increases.

1. Introduction

A fuel cell, in general, is an electrochemical energy device at which a fuel and oxidant – normally readily available oxygen from the ambient – react at two separate electrodes to convert the chemical energy into electrical energy. Unlike conventional power devices, i.e. gas turbines, steam turbines, and internal combustion engines, which are based on certain thermal cycles and use irreversible combustion to produce power, fuel cells have the potential to provide more power from a given supply of fuel and oxidant [1]. Not operating as a thermodynamic power cycle, the notion of maximum thermal efficiency imposed by the totally reversible Carnot machine is no longer valid for fuel cells.

Among the many different fuel cell types, direct methanol fuel cell (DMFC) is categorized as a low-temperature fuel cell with a proton conductive polymer electrolyte membrane. DMFCs are of great interest to provide power to many portable, low-temperature applications such as laptops and cell phones. They offer advantages of simple structure and instantaneous charging time in comparison to lithium-ion batteries [2,3]. However, there are still some barriers hindering mass product and commercialization of DMFCs, including water and methanol crossover through the membrane, and slow methanol oxidation kinetics at the anode. Achieving a higher energy density in DMFCs is of the highest priority. A higher efficiency, on the other hand, results in better and more efficient utilization of a certain amount of fuel supply. Among all kinds of analyses, an exergy study of DMFCs offers a more qualitative knowledge about the exergy flow in and out, as well as exergy destruction within the system by different kinds of irreversibilities.

Despite the large number of exergetic analyses conducted on high temperature solid-oxide fuel cells for stationary power generation [4–7], there are only few reported studies done on the exergetic analysis of low-temperature proton exchange membrane (PEM) fuel cells [8–12]. Hussain et al. [9] investigated the effect of operating conditions, i.e. temperature, pressure and air stoichiometry, on the energy and exergy efficiency of a power cycle using a PEM fuel cell. They found that the largest irreversibility occurs at the fuel cell stack. Ay et al. [10] studied the effect of operating conditions as well as membrane thickness on the exergetic performance of a PEM fuel cell. They reported a decrease in the exergy efficiency of the cell with an increase in the membrane thickness. A comparison was made between DMFC and methanol reforming of PEM fuel cell systems by Ishihara et al. [11] using exergy analysis, while the operating temperatures of both were kept at 80 °C. They noted that even though DMFCs do not need a fuel treatment system, their exergy efficiency could not go higher than that of reforming PEM fuel cells owing to higher irreversibility of methanol oxidation at the anode. Li et al. [12] investigated the exergetic efficiency of DMFCs, neglecting the effect of the cell temperature change. While they use an analytical solution to calculate the methanol crossover rate through the membrane, the cell voltage and electrochemistry are expressed by the other experimental correlations.

* Corresponding author. Tel.: +1 860 486 0419.
E-mail address: faghri@engr.uconn.edu (A. Faghri).

0378-7753/$ – see front matter © 2010 Elsevier B.V. All rights reserved.
doi:10.1016/j.jpowsour.2010.08.087

Nomenclature

a	specific area for oxidation/reduction, m^{-1}
ACL	anode catalyst layer
AGDL	anode gas diffusion layer
c	molar concentration, $mol\,m^{-3}$
$\bar{C}_p$	specific heat capacity, $J\,mol^{-1}\,K^{-1}$
CCL	cathode catalyst layer
CGDL	cathode gas diffusion layer
D	diffusivity, $m^2\,s^{-1}$
F	Faraday constant, 96,478 $C\,mol^{-1}$
Ex	exergy, J
$\bar{e}$	specific exergy, $J\,mol^{-1}$
g	gravity, $m\,s^{-2}$
$\bar{g}$	specific Gibbs exergy, $J\,mol^{-1}$
Gr	Grashof number
h	heat transfer coefficient, $W\,m^{-1}\,K^{-1}$
$\bar{h}$	specific enthalpy, $J\,mol^{-1}$
h_{fg}	heat of vaporization, $J\,kg^{-1}$
h_m	mass transfer coefficient, $m^{-2}\,s^{-1}$
$I_{H^+}(x)$	protonic current density, $A\,m^{-2}$
$I_{H^+}(0)$ or I_{H^+}	external circuit current density, $A\,m^{-2}$
I_p	parasitic current, $A\,m^{-2}$
I^{ref}_{o,O_2}	reduction exchange current density, $A\,m^{-2}$
$I^{ref}_{o,MeOH}$	oxidation exchange current density, $A\,m^{-2}$
K	permeability of porous media, m^2
k	thermal conductivity, $W\,m^{-1}\,K^{-1}$
L	length, m
$\dot{n}''$	molar flux, $mol\,m^{-2}\,s^{-1}$
n	number of moles
Nu	Nusselt number
n_d	electro-osmotic drag coefficient
p	pressure, Pa
Pr	Prandtl number
q'''	volumetric heat source, $J\,m^{-3}$
R	reaction rate, $A\,m^{-3}$
R_u	universal gas constant, $J\,(mol\,K)^{-1}$
$R_{contact}$	Ohmic contact resistance, $\Omega\,m^2$
$\bar{S}$	entropy, $J\,mol^{-1}\,K^{-1}$
S	liquid saturation
Sc	Schmidt number
Sh	Sherwood number
T	temperature, K
U	thermodynamic equilibrium voltage, V
x	coordinate, m, or mole fraction

Greek

α	transport coefficient
γ	reaction order of oxidation/reduction
ε	porosity of porous medium
η	over potential, V
θ	contact angle,°
μ	viscosity, $kg\,m^{-1}\,s^{-1}$
ρ	density, $kg\,m^{-3}$
σ	interfacial tension, $N\,m^{-1}$
σ_m	proton conductivity of the membrane phase, $\Omega^{-1}\,m^{-1}$
ϕ	carbon/membrane phase potential, V
ψ	relative humidity

Superscripts

ACL	anode catalyst layer
amb.	ambient
ch	chemical
e	environment
lim	limiting value
ref	reference value
sat.	saturated value
th-me	thermo-mechanical
∞	values in ambient air

Subscripts

a	anode
ACL	anode catalyst layer
AGDL	anode gas diffusion layer
amb.	ambient
c	cathode, or carbon phase
CO_2	carbon dioxide
cross	crossover
CCL	cathode catalyst layer
CGDL	cathode gas diffusion layer
e^-	electron
g	gas phase
H^+	proton
H_2O	water
l	liquid phase
m	membrane
MeOH	methanol
ox	oxidation
O_2	oxygen
rev.	reversible
sat	saturation value
T	temperature
v	vapor
0	ambient condition

To the best of authors' knowledge, none of the aforementioned research performed an exergetic analysis for a passive DMFC considering the temperature rise of the cell during the normal operation. While the operating temperature of an active DMFC is usually kept fixed at a constant value, the temperature in a passive DMFC is mainly governed by the electrochemical reactions at the catalyst layers and varies with the cell current density. Thus, providing an exergy analysis taking the cell temperature rise into account is inevitable. Furthermore, the analogy between heat and mass transport offers the opportunity to have a more comprehensive estimation of species concentrations at the cell boundaries which, in turn, results in a more comprehensive exergy analysis of the system in comparison to the previous studies [11,12]. The objectives of this study are two-fold: first, the fundamentals of the electrochemical kinetics, transport phenomena, and water and methanol crossovers are developed through an analytical model; then, the exergy analysis is utilized to provide a better understanding of all sources of entropy destruction inside the cell.

2. Mathematical models

The DMFC, shown in Fig. 1(a), operates in a completely passive mode and is considered as the thermodynamic system. Dilute methanol solution is supplied at a constant concentration in the fuel tank. Methanol and water diffuse through the anode gas diffusion layer (AGDL) to reach the anode catalyst layer (ACL) where the methanol will be oxidized in the presence of Pt–Ru catalysts to produce carbon dioxide, electrons, and protons. The anode electrode half reaction is:

$$CH_2OH + H_2O \rightarrow CO_2 + 6H^+ + 6e^- \quad (1)$$

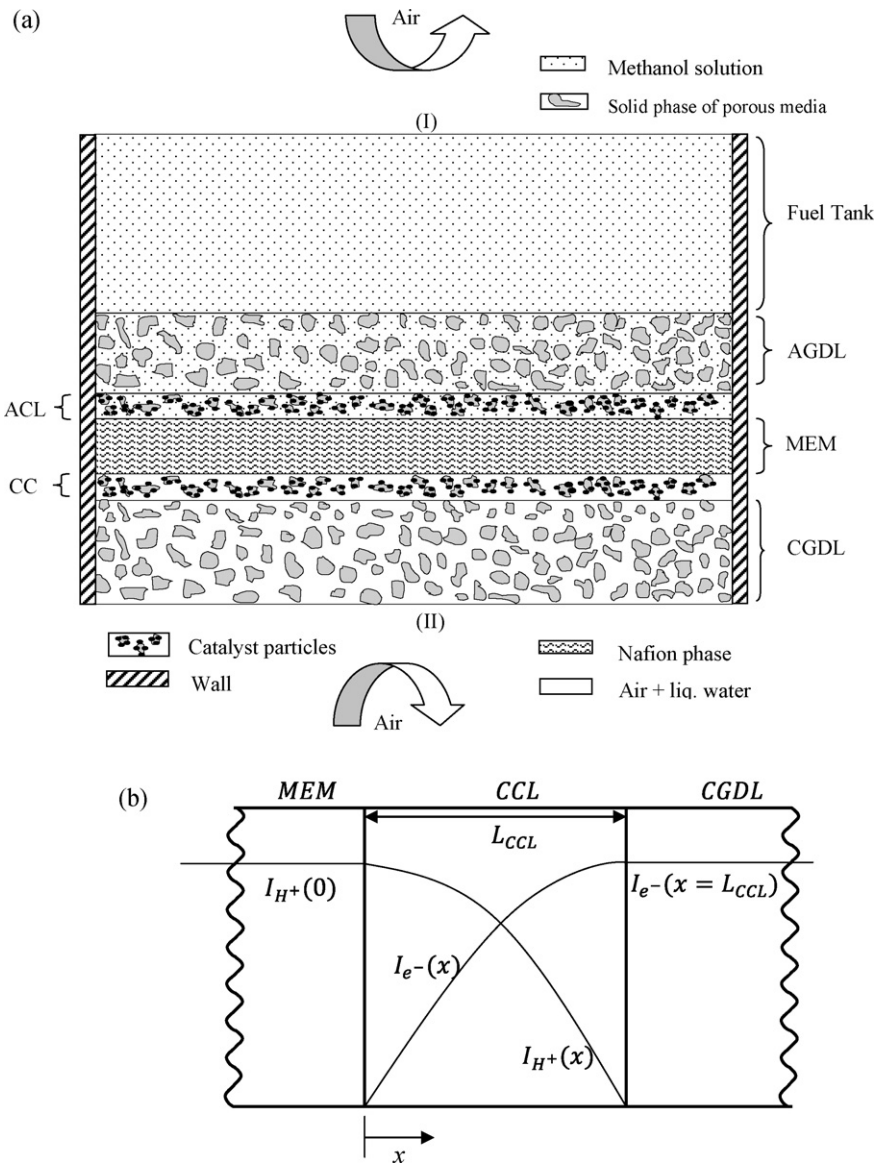

Fig. 1. (a) A schematic representation of a passive DMFC, and (b) protonic and electronic current density distributions at the CCL.

On the other side of the membrane at the cathode, oxygen reaches the cathode gas diffusion layer (CGDL) by natural convection from the ambient air. Then, it diffuses through the CGDL to the cathode catalyst layer (CCL). At the CCL, oxygen combines with protons and electrons traveling through the membrane and external circuit, respectively, to be reduced to liquid water, by the following reaction:

$$\frac{3}{2}O_2 + 6H^+ + 6e^- \rightarrow 3H_2O \quad (2)$$

In order to get the analytical solutions for the electrochemistry and distribution of the feeding species in the system, i.e. methanol, water, and oxygen, in conjunction with the cell temperature, the following assumptions are made:

- While the electronic and protonic current densities change along the catalyst layers, oxygen and methanol concentrations are assumed to be constant in these layers.
- The electrochemical reaction rates, both at the cathode and anode, are given by Tafel expressions.
- The electron conductivity of the carbon phase is assumed to be much higher than the proton conductivity of the membrane phase. As a result, the carbon phase potential, ϕ_c, is assumed to be constant at the catalyst layers.
- The convective transport of species is neglected through the entire domain.
- A constant concentration of methanol solution is supplied in the fuel tank.
- The membrane is fully saturated with dissolved water.
- Constant, average liquid saturations are assumed for both the anode and cathode.
- Temperature variation along the porous layers of the cell is neglected, thereby providing a lumped method for the energy equation.

2.1. Electrochemistry

To perform an exergetic balance on the DMFC, providing an analytical expression for the overpotential losses at the catalyst layers is necessary. In this study, a similar procedure as that of

[13] is taken to solve the electrochemistry inside the catalyst layers.

The reduction reaction rate of oxygen at the CCL is estimated by the following Tafel expression [14]:

$$R_{\text{red}} = (1-s)a_{\text{red}}1^{\text{ref}}_{0,\text{O}_2}\left(\frac{C_{\text{O}_2}}{C^{\text{ref}}_{\text{O}_2}}\right)^{\gamma_c}\exp\left(-\alpha_{\text{ref}}\eta_c\frac{F}{R_uT}\right) \quad (3)$$

where

$$\eta_c = \phi_c - \phi_m - U_{\text{O}_2} \quad (4)$$

Note that both the electronic (I_{e^-}) and protonic (I_{H^+}) current densities can be employed to calculate the overpotentials at the catalyst layers. However, since in this study an infinite electron conductivity for the carbon phase is assumed ($\sigma_c \to \infty$), all calculations are done based on the protonic current density. Considering the coordinate system shown in Fig. 1(b), the following relations can be written at the CCL:

$$\begin{cases} \dfrac{\partial I_{H^+}}{\partial x} = -R_{\text{red}} & 0 \le x \le L_{\text{CCL}} \\ I_{H^+} = -\sigma_m\dfrac{\partial\phi_m}{\partial x} \end{cases} \quad (5)$$

Substituting Eqs. (3) and (4) into Eq. (5), one obtains an explicit relation for the cathode overpotential in terms of cell current density and oxygen concentration at the CCL. A detailed mathematical manipulation is provided in Appendix A. The final solution for the cathode over-potential is as follows:

$$\bar{\eta}_c = \psi(\bar{I}_{H^+})\cdot\ln(\bar{I}_{H^+}) - \ln(\bar{R}_{0,c}) \quad (6)$$

with the notation that the bar sign refers to the non-dimensional parameters defined as follows:

$$\bar{I} = \frac{1}{(2\sigma_m R_uT/\alpha_cF)}, \quad \bar{R}_{0,c} = \frac{L_{\text{CCL}}\cdot(1-s)\cdot a_{\text{red}}I^{\text{ref}}_{0,\text{O}_2}}{(2\sigma_m R_uT/\alpha_cF)}\left(\frac{C_{\text{O}_2}}{C^{\text{ref}}_{\text{O}_2}}\right)^{\gamma_c},$$

$$\psi(\bar{I}_{H^+}) = 1 + \frac{1}{1+\bar{I}_{H^+}} \quad (7)$$

$\bar{I}_{H^+}$ denotes the protonic current density at the interface between the membrane and CCL (at $x=0$). Indeed, this is what is measured in the external circuit as the cell current density.

Likewise, Tafel kinetics is used to describe the methanol oxidation at the ACL, as follows:

$$R_{\text{ox}} = a_{\text{ox}}I^{\text{ref}}_{\text{o,MeOH}}\left(\frac{C_{\text{MeOH}}}{C^{\text{ref}}_{\text{MeOH}}}\right)^{\gamma_a}\exp\left(\alpha_{\text{ox}}\eta_a\frac{F}{R_uT}\right) \quad (8)$$

where

$$\eta_a = \phi_c - \phi_m - U_{\text{MeOH}} \quad (9)$$

The final expression for the anode overpotential is similar to that shown in Eq. (6):

$$\bar{\eta}_a = \psi(\bar{I}_{H^+})\cdot\ln(\bar{I}_{H^+}) - \ln(\bar{R}_{0,a}) \quad (10)$$

Note that for the methanol oxidation, the origin of the coordinate, $x=0$, starts at the interface between the membrane and ACL and ends at the interface between the ACL and AGDL. The non-dimensional parameters used for methanol oxidation are defined in the same fashion as those utilized for the oxygen reduction at the cathode side. The cell voltage, by definition, is the difference between the carbon phase potential of the anode ($\phi_{c,a}$) and the cathode ($\phi_{c,c}$):

$$V_{\text{cell}} = \phi_{c,c} - \phi_{c,a} \quad (11)$$

Protons flowing through the membrane encounter internal resistance causing a potential drop in membrane phase potential (ϕ_m):

$$R_{\text{resis},H^+,\text{mem}} = \phi_{m,a} - \phi_{m,c} = I_{H^+}\frac{\delta_m}{\sigma_m} \quad (12)$$

where δ_m is the membrane thickness and σ_m denotes the proton conductivity of the membrane. Through simple mathematical manipulation, Eq. (11) can be written as follows:

$$V_{\text{cell}} = U_{\text{O}_2} - I_{\text{MeOH}} - [\phi_{c,a} - \phi_{m,a} - U_{\text{MeOH}}] - [U_{\text{O}_2} - \phi_{c,c} + \phi_{m,c}] - R_{\text{resis},H^+,\text{mem}} \quad (13)$$

Taking into account the contact resistance of the current collector in the cell, and following the definitions of the cathode and the anode overpotentials given in Eqs. (4) and (9), Eq. (13) takes the following form:

$$V_{\text{cell}} = (U_{\text{O}_2} - U_{\text{MeOH}}) - \eta_a - |\eta_c| - I_{H^+}\left(R_{\text{contact}} + \frac{\delta_m}{\sigma_m}\right) \quad (14)$$

where the reversible cell voltage is calculated by the following expression [15]:

$$(U_{\text{O}_2} - U_{\text{MeOH}}) = V_{\text{rev.}} = V_{\text{rev.,298 K}} - (T_{\text{cell}} - 298)\times 1.4\times 10^{-4} \quad (15)$$

2.2. Species distribution

It follows from Eqs. (3) and (8) that the oxygen and methanol concentrations need to be calculated at the catalyst layers. Diffusion is deemed to be the dominant mechanism of species transport in the porous layers of the cell. Also, it is assumed that methanol crosses the membrane only by diffusion and electro-osmosis. Upon using these assumptions, the methanol concentration at the ACL is obtained by solving the following equation at the anode side:

$$\left|D_{\text{MeOH}}\frac{\partial C_{\text{MeOH}}}{\partial x}\right| = \frac{I_{H^+}}{6F} + \dot{n}''_{\text{cross,MeOH}} \quad (16)$$

which can be rewritten as:

$$\frac{C^{\infty}_{\text{MeOH}} - C^{\text{ACL}}_{\text{MeOH}}}{L_{\text{AGDL}}} = \frac{1}{D_{\text{MeOH}}}\left[\frac{I_{H^+}}{6F} + D_{\text{MeOH,m}}\frac{C^{\text{ACL}}_{\text{MeOH}}}{L_m} + n_d\frac{I_{H^+}}{F}\cdot\frac{C^{\text{ACL}}_{\text{MeOH}}}{C^{\text{ACL}}_{\text{MeOH}} + C^{\text{ACL}}_{\text{H}_2\text{O}}}\right] \quad (17)$$

For the sake of convenience, the following non-dimensional parameters are defined:

$$I^{\text{lim}}_{\text{MeOH,a}} = 6F\frac{C^{\infty}_{\text{MeOH}}D_{\text{MeOH}}}{L_{\text{AGDL}}}, \; I^{\text{lim}}_{\text{H}_2\text{O,a}} = 6F\frac{C^{\infty}_{\text{H}_2\text{O}}D_{\text{MeOH}}}{L_{\text{AGDL}}},$$

$$\beta = \frac{D_{\text{MeOH,m}}}{L_m}\cdot\frac{L_{\text{AGDL}}}{D_{\text{MeOH}}}, \; \xi_{\text{MeOH}} = \frac{I_{H^+}}{I^{\text{lim}}_{\text{MeOH,a}}}, \; \xi_{\text{H}_2\text{O}} = \frac{I_{H^+}}{I^{\text{lim}}_{\text{H}_2\text{O,a}}},$$

$$\theta = \frac{C^{\text{ACL}}_{\text{H}_2\text{O}}}{C^{\infty}_{\text{MeOH}}}, \; I_{\text{H}_2\text{O,ACL}} = F\frac{C^{\text{ACL}}_{\text{H}_2\text{O}}D_{\text{MeOH}}}{L_{\text{AGDL}}}$$

Upon using the above non-dimensional parameters, one can solve Eq. (17) for the positive $C^{\text{ACL}}_{\text{MeOH}}$, as follows:

$$C^{\text{ACL}}_{\text{MeOH}} = \begin{cases} \dfrac{C^{\infty}_{\text{MeOH}}}{2(1+\beta)}[\chi + \sqrt{\chi^2 + (4(1-\xi_{\text{MeOH}})(1+\beta)\theta)}] & \xi_{\text{MeOH}} < 1 \\ 0 & \xi_{\text{MeOH}} = 1 \end{cases} \quad (18)$$

with the notation that:

$$x = 1 - (1 + 6n_d)\xi_{MeOH} - (1 + \beta)\theta$$

It should be pointed out that θ in Eq. (18) is still unknown, which requires solving for the water concentration at the ACL. Considering electro-osmotic drag to be the only mechanism of water crossover through the membrane, the concentration of liquid water at the ACL is obtained as the following:

$$\frac{C^{\infty}_{H_2O} - C^{ACL}_{H_2O}}{L_{AGDL}} = \frac{1}{D_{H_2O}}\left[\frac{I_{H^+}}{6F} + n_d\frac{I_{H^+}}{F}\cdot\frac{C^{ACL}_{H_2O}}{C^{ACL}_{MeOH} + C^{ACL}_{H_2O}}\right] \quad (19)$$

Upon using the non-dimensional parameter, $Z = C^{ACL}_{H_2O}/C^{\infty}_{H_2O}$, the relation for Z appears as:

$$1 - Z = \xi_{H_2O}\left[1 + \frac{12\cdot n_d\cdot(1+\beta)Z}{(2(1+\beta)Z) + \left(\frac{C^{\infty}_{MeOH}}{C^{\infty}_{H_2O}}\left(\chi + \sqrt{\chi^2 + (4(1-\xi_{MeOH})(1+\beta)\theta)}\right)\right)}\right] \quad (20)$$

Since there is no closed-form solution for Z, Eq. (20) can iteratively be solved for Z. Note that if the concentration of methanol at the ACL was neglected compared to that of water at the ACL, Z would have the following explicit expression:

$$Z = 1 - \xi_{H_2O}(1 + 6n_d) \quad (21)$$

Eq. (21) can now be used as the initial guess to solve Eq. (20). Finally, knowing the methanol crossover through the membrane, the oxygen concentration at the CCL is calculated as follows:

$$D_{O_2}\frac{C^{\infty}_{O_2} - C^{CCL}_{O_2}}{L_{CGDL}} = \frac{I_{H^+}}{4F} + \frac{3}{2}\dot{n}''_{cross,MeOH} \quad (22)$$

2.3. Cell temperature

Providing a model that can predict the cell temperature during operation is vital for an exergy study of a passive DMFC. However, since the total thickness of the five main porous layers of the DMFC is small, the spatial distribution of the temperature can be neglected [16,17]. It is further assumed that heat is only generated at the CCL and ACL due to electrochemical reactions. The volumetric heat generation at the ACL due to methanol oxidation is:

$$q'''_{ACL} = I_{H^+} + \frac{\eta_a - (T\cdot\Delta\bar{S}a/6F)}{L_{ACL}} \quad (23)$$

where η_a is the anode overpotential corresponding to the value of I_{H^+} as the cell current. At the CCL, oxygen has to be reduced in the presence of both electrons traveling through the external circuit and electrons released by the chemical reaction of migrated methanol through the membrane. Considering this notion, the heat source term at the CCL is as follows:

$$q'''_{CCL} = (I_{H^+} + I_P)\frac{\eta_c - (T\cdot\Delta\bar{S}_C/6F)}{L_{CCL}} - I_P\frac{T\cdot\Delta\bar{S}_a}{6F\cdot L_{CCL}} \quad (24)$$

where I_p denotes the crossover current and equals:

$$I_p = 6F\cdot\dot{n}''_{cross,MeOH} \quad (25)$$

The Peltier effect, $(T\Delta\bar{S}/6F)$, for the anode and cathode half reactions are calculated as the following:

$$\left(\frac{T\Delta\bar{S}}{6F}\right)_{\alpha} = \frac{T}{6F}(\bar{S}_{CO_2} + 6\bar{S}_{H^+} + 6\bar{S}_{e^-} - \bar{S}_{MeOH} - \bar{S}_{H_2O}) \quad (26)$$

$$\left(\frac{T\Delta\bar{S}}{6F}\right)_{c} = \frac{T}{6F}\left(3\bar{S}_{H_2O} + \frac{3}{2}\bar{S}_{O_2} - 6\bar{S}_{H^+} - 6\bar{S}_{e^-}\right) \quad (27)$$

Since the local distribution of the temperature inside the cell is neglected, by adding up Eqs. (23) and (24), one concludes that the entropy values for electron and proton will drop out from the heat source term. Therefore, only the entropy change of the overall cell reaction is required. However, it worth it to note that a conventional entropy system may be used to calculate the entropy of charged particles in half-cell reactions [18–20]. Lampinen and Fomino [20] proposed a semi-absolute entropy system by which problems involving non-charged and charged species can be considered.

Generated heat at the catalyst layers is transferred to the environment by natural convection in conjunction with the evaporation of condensable species in the system. Thus, the mass transport has to be taken into account. It is a common practice in thermal science to use the analogy between heat and mass transport to predict the mass transport based on the knowledge of heat transport phenomenon as a zero-order approximation. The heat and mass transfer coefficients at interface (I) in Fig. 1(a) are taken from the natural convection correlations on a horizontal surface facing up [21].

$$Nu = 0.54(Gr\cdot Pr)^{0.25}, \quad Nu = \frac{hL}{k} \quad (28)$$

$$Sh = 0.54(Gr\cdot Sc)^{0.25}, \quad Sh = \frac{h_m L}{\rho D} \quad (29)$$

$$Gr = \frac{g\rho|\Delta\rho|L^3}{\mu^2} \quad (30)$$

with the notation that L is the characteristic length and is chosen as the distance between the two vertical solid walls in Fig. 1(a). The heat and mass transfer coefficients at the air breathing surface (interface (II)) are calculated in a similar fashion for a horizontal surface facing down. The coefficients for this interface are as follows [21]:

$$Nu = 0.27(Gr\cdot Pr)^{0.25}, \quad Nu = \frac{hL}{k} \quad (31)$$

$$Sh = 0.27(Gr\cdot Sc)^{0.25}, \quad Sh = \frac{h_m L}{\rho D} \quad (32)$$

Evaporation is the other mechanism that cools the cell down. Since the entire crossover methanol is consumed at the CCL, methanol evaporation can only occur at the anode side. Assuming that the methanol and water are saturated at interface (I), the molar flux of evaporated methanol and water at this surface are calculated as:

$$\dot{n}''_{MeOh,v,a} = h_{m,MeOH}(C^{sat.}_{MeOH} - C^{amb.}_{MeOH}) \quad (33)$$

$$\dot{n}''_{H_2O,v,a} = h_{m,H_2O}(C^{sat.}_{H_2O} - C^{amb.}_{H_2O}) \quad (34)$$

where superscript amb. pertains to the ambient condition. While the concentration of methanol vapor at the ambient is nearly zero, the water vapor concentration is calculated based on the relative humidity of the ambient, $\psi^{amb.}$, as follows:

$$C^{amb.}_{H_2O} = \frac{\psi^{amb.}\cdot p^{sat.}_{H_2O}(T^{amb.})}{R_u\cdot T^{amb.}} \quad (35)$$

However, assuming saturation condition for the water vapor at the cathode end of the cell may result in over-predicting the evaporated water from the cell for small current densities. There are

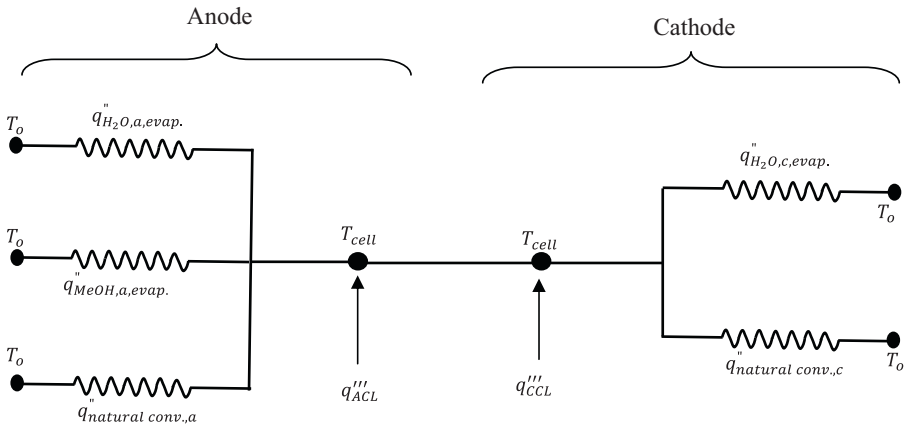

Fig. 2. Thermal resistance network for a passive DMFC.

two sources of liquid water at the cathode side; migrated water through the membrane by the electro-osmotic drag, and the water generation due to the reduction of oxygen at the CCL. Both of these water sources are directly proportional to the cell current density. In this study, based on numerical results [14,16,17], it is assumed that 70% of the existing water at the cathode is evaporated to the ambient, and rest of that is evacuated in the liquid form.

Carbon dioxide bubbles at the anode also carry some of the evaporated water and methanol. To have a first-order estimation, the gas pressure at the anode has to be calculated. Numerical studies [14,16,17] revealed that the liquid pressure at the anode as well as the gas pressure at the cathode is nearly equal to the atmospheric pressure. Thus, assuming a constant liquid saturation, the gas pressure at the anode is obtained as follows:

$$p_{g,a} = p_{l,a} + \sigma \cos(\theta)\left(\frac{\varepsilon}{k}\right)^{0.5} J(s) \tag{36}$$

The Leverette function, $J(s)$, is a function of liquid saturation, wettability, and morphological properties of the porous material. However, in this study, Udell's correlation [22] obtained from geological porous media is adopted to evaluate $J(s)$:

$$J(s) = \begin{cases} 1.42(1-s) - 2.12(1-s)^2 + 1.26(1-s)^3 & \text{if } \theta < 90^\circ \\ 1.42s - 2.12s^2 + 1.26s^3 & \text{if } \theta > 90^\circ \end{cases} \tag{37}$$

Assuming that the water and methanol vapor inside the carbon dioxide bubbles are in a saturated state, the following relation is used to calculate the partial pressure of CO_2 inside the bubbles:

$$p_{g,CO_2} = p_{g,a} - p^{sat.}_{MeOH,v} - p^{sat.}_{H_2O,v} \tag{38}$$

Knowing the rate of CO_2 generation at the ACL, and upon using the ideal gas relation, the amount of evaporated water and methanol carried by the CO_2 bubbles are obtained as the following:

$$\dot{n}''_{MeOH,v,bubble,a} = \frac{I_{H^+}}{6F}\frac{p^{sat.}_{MeOH,v}}{p_{g,CO_2}} \tag{39}$$

$$\dot{n}''_{H_2O,v,bubble,a} = \frac{I_{H^+}}{6F}\frac{p^{sat.}_{H_2O,v}}{p_{g,CO_2}} \tag{40}$$

The total heat removal by the evaporation of water and methanol in the domain are as follows:

$$q''_{H_2O,evap.} = \left(\dot{n}''_{H_2O,v,bubbl,a} + \dot{n}''_{H_2O,v,a} + \dot{n}''_{H_2O,v,c}\right) h_{fg,H_2O} \tag{41}$$

$$q''_{MeOH,evap.} = (\dot{n}''_{MeOH,v,bubbl,a} + \dot{n}''_{MeOH,v,a}) h_{fg,MeOH} \tag{42}$$

Fig. 2 displays the thermal resistance network involving heat generation and heat removal at both the anode and cathode. Note that an iterative manner, with an appropriate under-relaxation, has to be taken to get the converged value of the cell temperature at each individual current density of the cell.

2.4. Exergy balance

The second law of thermodynamics puts restrictions on the efficiency of transforming one form of energy to another. As a result, exergy is a property that quantifies the potential for maximum work. Unlike energy which is conserved in every process, exergy can be destroyed by the irreversibilities or be transferred to and from thermodynamic systems. Depicted in Fig. 3(a) is a schematic of all the components with their corresponding pressure and temperature, in a DMFC during the passive operation. As shown, there are a total of three components coming into the system and six dif-

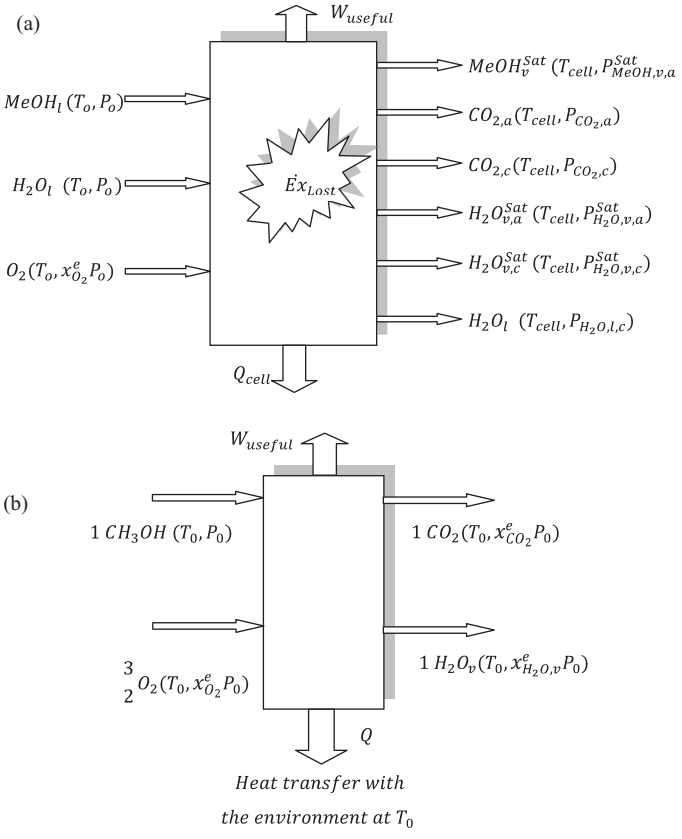

Fig. 3. A schematic representation of (a) all components coming into the system (DMFC) and going out, with their corresponding pressure and temperature, and (b) the reactor used to introduce the chemical exergy of liquid methanol

Table 1
Exergy reference environment.

Thermo-mechanical exergy reference environment	
T_0	298 K
P_0	101,325 Pa

Chemical exergy reference environment	
Gas phase species	Molar fraction
N_2	0.7560
O_2	0.2034
H_2O (vapor)	$f(\psi)$, $\psi = 70\%$
CO_2	0.0003

ferent species going out. While the cell produces some electrical work and exchanges heat to the environment, some of the input exergy is destroyed due to irreversibilities. Looking at Fig. 3, the exergy balance of a DMFC may be written as follows:

$$\sum \dot{E}x_{\text{mass,in}} = \sum \dot{E}x_{\text{mass,out}} + \sum \dot{E}x_{\text{work}} + \sum \dot{E}x_{\text{heat}} + \dot{E}x_{\text{lost}} \tag{43}$$

with the notation that:

$$\sum \dot{E}x_{\text{mass,in}} = (\dot{n}'' \cdot \bar{e})_{\text{MeOH,l}} + (\dot{n}'' \cdot \bar{e})_{\text{O}_2} + (\dot{n}'' \cdot \bar{e})_{\text{H}_2\text{O,l}} \tag{44}$$

$$\sum \dot{E}x_{\text{mass,out}} = (\dot{n} \cdot \bar{e})_{\text{H}_2\text{O,l}} + (\dot{n}'' \cdot \bar{e})_{\text{CO}_2} + (\dot{n}'' \cdot \bar{e})_{\text{H}_2\text{O,v}} + (\dot{n}'' \cdot \bar{e})_{\text{MeOH,v}} \tag{45}$$

$$\sum \dot{E}x_{\text{heat}} = q'' \left(1 - \frac{T_0}{T_{\text{cell}}}\right) \tag{46}$$

For a reacting system, the total exergy consists of both *thermo-mechanical* and *chemical* exergies. Calculating the chemical exergy requires quantifying the molar fractions of all available species in the exergy reference environment, which is presented in Table 1. Assuming that the partial pressure of the species of interest in the reference environment is P_0, the thermo-mechanical exergy, by definition, is the maximum theoretical work obtainable from that species of property of (T, P) as it comes into thermal and mechanical equilibrium with the reference environment. The general equation for thermo-mechanical exergy is expressed as the following:

$$\left(\bar{e}^{\text{th-me}}\right)_{(T,p)} = (\bar{h} - T_0\bar{s})_{T,p} - (\bar{h}_0 - T_0\bar{s}_0)_{(T_0,p_0)} \tag{47}$$

where the ideal gas relations are used to calculate the enthalpy and entropy difference for all gaseous species in the domain.

On the other hand, chemical exergy is the maximum theoretical work that can be produced by a virtual Carnot machine in which a substance of interest enters at (T_0, P_0) and completely expands or reacts to produce the environmental components at $(T_0, x_i P_0)$, where x_i denotes the molar fraction of that component in the environment. It should be pointed out that for the liquid state of the condensable species in the system, i.e. water and methanol, the chemical exergy is defined as the maximum theoretical work that a Carnot machine can produce as these components enter the machine at (T_0, P_0) and exit at $(T_0, x_i P_0)$, where x_i is the molar fraction of the vapor state of corresponding species in the environment.

2.4.1. Exergy flow into the system

Since methanol enters the cell at (T_0, P_0) in the liquid form, the contribution of thermo-mechanical exergy is zero. However, the chemical exergy is not zero. Fig. 3(b) shows how one mole of liquid methanol reacts with the environmental component of oxygen to produce other corresponding environmental components. The maximum work obtainable from this system, chemical exergy, is equal to the Gibbs energy difference of the reactants and products, as follows:

$$\begin{aligned}\bar{e}_{\text{MeOH,in}} &= (\bar{e}^{\text{ch}})_{(T_0,P_0)} = (\textstyle\sum \bar{g}_{\text{R}} - \sum \bar{g}_{\text{P}}) \\ &= \left(\left[\bar{g}_{\text{MeOH,l}} + \frac{3}{2}\bar{g}_{\text{CO}_2} - \bar{g}_{\text{CO}_2} - 2\bar{g}_{\text{H}_2\text{O,v}}\right]_{(T_0,P_0)} \right. \\ &\quad \left. + R_{\text{u}}T_0 \ln\left(\frac{x_{\text{O}_2}^{\text{e}2}}{x_{\text{H}_2\text{O,v}}^{\text{e}2} \cdot x_{\text{CO}_2}^{\text{e}}}\right)\right)\end{aligned} \tag{48}$$

where the Gibbs energy of oxygen at the atmospheric conditions is zero.

Since the water in the exergy reference environment exists in a vapor form, liquid water carries some chemical exergy into the system, as:

$$\begin{aligned}\bar{e}_{\text{H}_2\text{O,l,in}} &= (\bar{e}^{\text{th-me}})_{(T_0,P_0)} + (\bar{e}^{\text{ch}})_{(T_0,P_0)} \\ &= 0 + \left([\bar{g}_{\text{H}_2\text{O,l}} - \bar{g}_{\text{H}_2\text{O,v}}]_{(T_0,P_0)} + R_{\text{u}}T_0 \ln\left(\frac{1}{x_{\text{H}_2\text{O,v}}^{\text{e}}}\right)\right)\end{aligned} \tag{49}$$

Note that since the oxygen enters the system as an environmental component, both its thermo-mechanical and chemical exergies are zero.

2.4.2. Exergy flow out of the system

Exergy of carbon dioxide going out of the system at the anode is obtained as follows:

$$\begin{aligned}\bar{e}_{\text{CO}_2,\text{a,out}} &= (\bar{e}^{\text{th-me}})_{(T_0,x_{\text{CO}_2,\text{a}}P_0)} + (\bar{e}^{\text{ch}})_{(T_0,P_0)} \\ &= \left[(\bar{C}_{p,\text{CO}_2}(T_{\text{cell}} - T_0)) - T_0\left(\bar{C}_{p,\text{CO}_2} \ln\left(\frac{T_{\text{cell}}}{T_0}\right)\right.\right. \\ &\quad \left.\left. - R_{\text{u}} \ln\left(\frac{p_{\text{CO}_2,\text{a}}}{p_{\text{o}}}\right)\right)\right] + \left[R_{\text{u}}T_0 \ln\left(\frac{1}{x_{\text{CO}_2}^{\text{e}}}\right)\right]\end{aligned} \tag{50}$$

Exergy of CO_2 at the cathode is calculated in a similar fashion. Water vapor also takes some exergy out of the system. The exergy of water vapor at the anode is obtained as:

$$\begin{aligned}\bar{e}_{\text{H}_2\text{O,v,a,out}} &= \left[(\bar{C}_{p,\text{H}_2\text{O,v}}(T_{\text{cell}} - T_0)) - T_0\left(\bar{C}_{p,\text{H}_2\text{O,v}} \ln\left(\frac{T_{\text{Cell}}}{T_0}\right)\right.\right. \\ &\quad \left.\left. - R_{\text{u}} \ln\left(\frac{p\text{H}_2\text{O, v, a}}{p_{\text{o}}}\right)\right)\right] + \left[R_{\text{u}}T_{\text{o}} \ln\left(\frac{1}{x_{\text{H}_2\text{O,v}}^{\text{e}}}\right)\right]\end{aligned} \tag{51}$$

Exergy taken out of the system by methanol vapor at the anode can be calculated in a same fashion as of Eq. (48) with the exception of using the vapor phase Gibbs energy for the methanol. The chemical exergy of liquid water exiting the cathode side at $(T_{\text{cell}}, P_{\text{l,c}})$ is the same as that of liquid water at the anode, and therefore, Eq. (49) can be used for this purpose. However, the thermo-mechanical exergy has to be calculated using Eq. (47) assuming an incompressible liquid. Assuming a constant liquid saturation at the cathode, the cathode liquid pressure is calculated.

3. Results and discussion

Physicochemical properties, as well as cell geometries and operating conditions, are given in Tables 2 and 3, respectively. All electrochemical and physical parameters in the present model are calibrated using the polarization experimental data of [23]. As shown in Fig. 4(a), a good agreement between the experimental data and results obtained by the present analytical model is seen for two different methanol solutions in the tank. Since

a non-isothermal model is presented, a validation for the predicted temperature is necessary. Depicted in Fig. 4(b) is the comparison between the cell temperature reported by [23] and that obtained by the present model. It should be pointed out that since [23] used a tank with a finite capacity, the cell temperature never reaches the steady state value. The experimental cell temperature data comprises the cell temperature after the first 15 min of each cell load being applied. Temperatures obtained by the present model are within 2% of the experimental data.

Of particular interest in the DMFC is the crossover of water and methanol through the membrane. There are two mechanisms of methanol crossover considered in this study; electro-osmosis and diffusion, as shown in Fig. 5(a). While the diffusive mechanism of methanol crossover decreases monotonically versus cell current density, the electro-osmotic drag of methanol shows an increase at low currents and then, after reaching a certain pick point, starts decreasing. The slope of the increase in the electro-osmotic drag of methanol at low currents increases as the methanol solution in the tank becomes more concentrated. Summation of these two mechanisms is the total methanol crossover flux through the membrane which is shown in Fig. 5(b). While for 1 M and 2 M solutions in the tank the total flux of methanol monotonically reduces as the current increases, methanol crossover for 3 M solution first shows an increase at low current densities and then decreases after reaching a maximum value. The underlying rationale for this behavior is that the methanol concentration at the ACL decreases as the cell current increases (Eq. (17)). Although the electro-osmotic crossover of methanol is linearly proportional to the cell current density, the reduction of $C_{MeOH,ACL}$ is the dominant factor in decreasing the total methanol crossover as the cell current density increases for methanol feeding concentrations lower than 3 M. The variation of the methanol crossover versus cell current density for different methanol solutions are in good

Table 2
Physicochemical properties.

Parameters		Symbols	Value	Unit	Ref.
Diffusivities, liquid	MeOH in water	D_{MeOH}	$1.58\times10^{-9}e^{0.02623(T-298)}(\varepsilon.s)^{\tau}$	$m^2\,s^{-1}$	[26]
	MeOH in Nafion	$D_{MeOH,m}$	$4.9\times10^{-10}e^{\left[2436\left(\frac{1}{333}-\frac{1}{T}\right)\right]}(\varepsilon.s)^{\tau}$	$m^2\,s^{-1}$	[26]
Diffusivities, gas		D_{g,O_2}	$1.775\times10^{-5}\left(\frac{T}{273.15}\right)^{1.823}(\varepsilon.(1-s))^{\tau}$	$m^2\,s^{-1}$	[27]
Electron conductivity in carbon phase		σ_c	4000	$\Omega^{-1}m^{-1}$	[28]
Proton conductivity in membrane phase		σ_m	3	$\Omega^{-1}m^{-1}$	
Heat capacity		$\bar{C}_{p,l,H_2O}$	$\left(\begin{matrix}-2.667\times10^{-7}T^3+2.68\times10^{-4}T^2+\\-8.92\times10^{-2}T+1.4023\times10^{1}\end{matrix}\right)\times18$	$J\,mol^{-1}\,K^{-1}$	[21] fitted
		$\bar{C}_{p,l,MeOH}$	79.5	$J\,mol^{-1}\,K^{-1}$	
		$\bar{C}_{p,H_2}/R_u$	$\left(\begin{matrix}-1.812\times10^{-12}T^4+5.521\times10^{-9}T^3\\-5.8\times10^{-6}T^2+2.67\times10^{-3}T+3.057\end{matrix}\right)$	--	
		$\bar{C}_{p,O_2}/R_u$	$\left(\begin{matrix}2.156\times10^{-12}T^4-6.764\times10^{-9}T^3+\\7.055\times10^{-6}T^2-1.878\times10^{-3}T+3.626\end{matrix}\right)$	--	
		$\bar{C}_{p,CO_2}/R_u$	$\left(\begin{matrix}2.002\times10^{-9}T^3-6.607\times10^{-6}T^2\\+8.735\times10^{-3}T+2.401\end{matrix}\right)$	--	
		$\bar{C}_{p,g,H_2O}/R_u$	$\left(\begin{matrix}0.807\times10^{-12}T^4-2.964\times10^{-9}T^3+\\4.152\times10^{-6}T^2-1.108\times10^{-3}T+4.07\end{matrix}\right)$	--	
		$\bar{C}_{p,g,MeOH}$	$\left(\begin{matrix}-2.0833\times10^{-7}T^3+1.895\times10^{-4}T^2\\-5.385\times10^{-2}T+6.187767\end{matrix}\right)\times32$	$J\,mol^{-1}\,K^{-1}$	
Absolute entropy (1 *atm*, 298 K)	Liquid phase	$\bar{s}^o_{l,MeOH}$	126.8	$J\,mol^{-1}\,K^{-1}$	
		$\bar{s}^o_{l,H_2O}$	69.95	$J\,mol^{-1}\,K^{-1}$	
	Gas phase	$\bar{s}^o_{CO_2}$	213.685	$J\,mol^{-1}\,K^{-1}$	
		$\bar{s}^o_{O_2}$	205.033	$J\,mol^{-1}\,K^{-1}$	
		$\bar{s}^o_{H_2}$	128.7	$J\,mol^{-1}\,K^{-1}$	
Gibbs function of formation (1 *atm*, 298 K)	Liquid phase	$\bar{g}^o_{l,MeOH}$	−166290	$J\,mol^{-1}$	[1]
		$\bar{g}^o_{l,H_2O}$	−237180	$J\,mol^{-1}$	
	Gas phase	$\bar{g}^o_{CO_2}$	−394380	$J\,mol^{-1}$	
		$\bar{g}^o_{v,H_2O}$	−228590	$J\,mol^{-1}$	
		$\bar{g}^o_{l,MeOH}$	−162140	$J\,mol^{-1}$	
Electro-osmotic drag coefficients		n_d	2.5	-	[27]
Henry law constant for methanol		$k_{H,MeOH}$	$0.096e^{[0.04511(T-273)]}$	*atm*	[27]

and

Table 2 (*Continued*)

The saturation pressure of pure water	$log_{10}^{p_{g,sat,H_2O}^{pure}}$	$-2.1794 + 0.02953(T-273.15) - 9.1837\times10^{-5}(T-273.15)^2 + 1.4454\times10^{-7}(T-273.15)^3$	atm	[26]
Latent heat of evaporation ($20 < T(^oC) < 80$)	$h_{fg,MeOH}$	$\left(\frac{-1.292T^3 + 76.25T^2 - }{14558.3T + 1.2182\times10^7}\right)\times10^{-1}$	$J\,kg^{-1}$	[26]
	h_{fg,H_2O}	$\left(\frac{-1.25\times10^{-1}T^3 + 4.9997T^2 - }{23.6\times10^3T + 2.5009\times10^7}\right)\times10^{-1}$	$J\,kg^{-1}$	
Cell thermodynamic voltage	$V_{rev.,298\,K}$	1.216	V	[15]
Transfer coefficient of anode	α_a	1.	-	Assumed
Transfer coefficient of cathode	α_c	1.1	-	Assumed
Anode exchange current density	$I_{o,MeOH}^{ref}$	$94.25e^{\left[\frac{35570}{R_u}\left(\frac{1}{353}-\frac{1}{T}\right)\right]}$	$A\,m^{-2}$	[26]
Cathode exchange current density	I_{o,O_2}^{ref}	$0.04222e^{\left[\frac{73200}{R_u}\left(\frac{1}{353}-\frac{1}{T}\right)\right]}$	$A\,m^{-2}$	[26]
Specific area	a_{ox}	106.1	m^{-1}	Assumed
	a_{red}	5000	m^{-1}	
Anode reference concentration	$C_{l,MeOH}^{ref}$	10000	$mol.m^{-3}$	Assumed
Cathode reference concentration	$C_{O_2}^{ref}$	$C_{O_2}^{env.}$	$mol.m^{-3}$	Assumed
Surface tension ($10 < T(^oC) < 75$)	σ_{H_2O}	$\left(\frac{9.3\times10^{-3}T^3 - 3.96T^2}{-1363.8T + 756325}\right)\times10^{-7}$	$N\,m^{-1}$	[19]
	σ_{MeOH}	$\left(\frac{3.3\times10^{-2}T^2 - 774.5T}{+240041.67}\right)\times10^{-7}$	$N\,m^{-1}$	Fitted
Liquid water density	ρ_{l,H_2O}	$exp\left(\begin{matrix}6.9094 - 2.0146\times10^{-5}(T-273) \\ -5.9868\times10^{-6}(T-273)^2 + \\ 2.5921\times10^{-8}(T-273)^3 - \\ 9.3244\times10^{-11}(T-273)^4 + \\ 1.2103\times10^{-13}(T-273)^5\end{matrix}\right)$	$Kg.m^{-3}$	[28]
Liquid methanol density	$\rho_{l,MeOH}$	$244.4\times0.224^{\left(-\left(1-\frac{T}{513}\right)^{\frac{2}{7}}\right)}$	$Kg.m^{-3}$	[29]

agreement with that has been reported by Meyers and Newman [24].

In DMFCs, methanol crossover is strongly interconnected with the water crossover. DMFCs using highly concentrated methanol can achieve a low methanol crossover, if the water crossover is limited [14]. Since in this study only the electro-osmotic drag of water through the membrane is considered, an increase in water crossover is observed as the cell current increases. If the molar fraction of liquid water at the ACL is approximated to be unity, as is the case for most analytical solutions such as [12,13], there would be no difference in water crossover for different methanol concentrations in the tank. However, Fig. 6(a) illustrates that the molar fraction of liquid water at the ACL is less than unity, especially for lower cell current densities and higher methanol concentrations in the tank. Fig. 6(b) depicts that the water concentration at the ACL reduces as the current density increases due to higher electrochemical consumption and water crossover through the membrane. As expected, the water concentration at the ACL is lower, when the methanol solution in the tank is more concentrated.

As previously noted, there are three components carrying chemical exergy into the system; oxygen at the cathode, and liquid water and methanol at the anode. However, since it is assumed that the oxygen at the cathode is supplied by the environment, the total exergy of oxygen always equals zero. Fig. 7 shows the total exergy flow of liquid water and methanol at the anode, which is completely contributed by the chemical exergy. As expected, the chemical exergy of liquid methanol flowing into the system is several orders of magnitude greater than that of liquid water. It is observed that the total flow of exergy increases as the cell current density increases, which is a direct result of a higher mass flow rate and cell temperature at larger current densities. Exergy supplied by the liquid methanol to the system is one order of magnitude larger than that by the liquid water.

On the other hand, there are a total of six components flowing out of the system, among which methanol vapor at the anode carries the highest exergy out of the cell. Methanol evaporation, either from the top of the anode tank (interface (I)) or into the CO_2 bubbles, strongly depends on the cell temperature and methanol concentration. As shown in Fig. 8, the exergy of methanol vapor for 3 M methanol solution is larger than that for 1 M. While the CO_2 production and its exergy flow at the cathode are proportional to the methanol crossover through the membrane and tend to decrease at

Table 3
Cell geometric dimensions and operating parameters.

Parameters	Symbols	Value	Unit
Anode gas diffusion layer thickness	δ_{AGDL}	0.26	mm
Anode catalyst layer thickness	δ_{ACL}	0.02	mm
Membrane thickness (Nafion 115)	δ_{MEM}	0.125	mm
Cathode catalyst layer thickness	δ_{CCL}	0.02	mm
Cathode gas diffusion layer thickness	δ_{CGDL}	0.26	mm
Permeability	K	2×10^{-12}	m^2
Porosity	ε	0.6	–
Contact angle	θ	120	–
Anode liquid saturation	s_a	0.8	–
Cathode liquid saturation	s_c	0.1	–

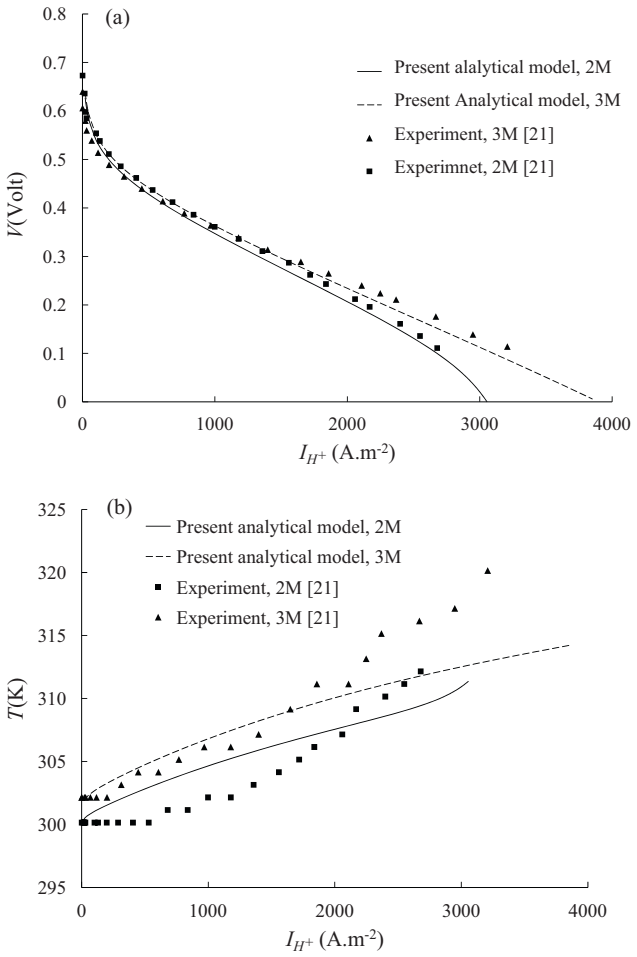

Fig. 4. (a) Polarization curve, and (b) the cell temperature versus current density, for two different methanol solutions in the tank.

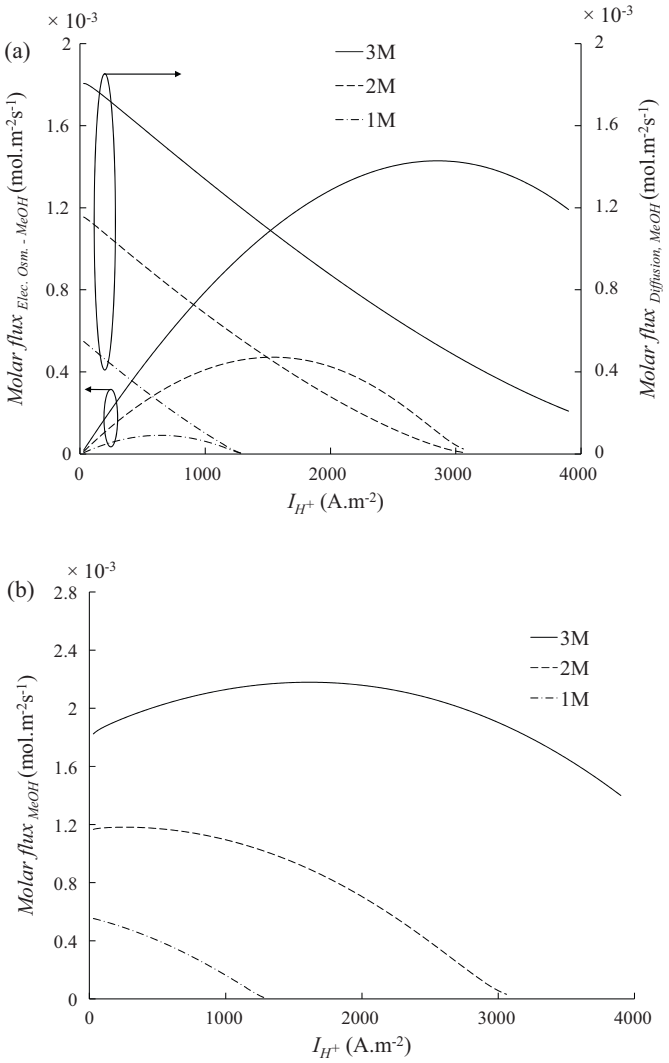

Fig. 5. (a) The electro-osmotic drag and diffusive transport of methanol through the membrane, and (b) total methanol crossover flux for three distinct methanol concentrations in the tank.

high current densities, exergy flow of CO_2 at the anode monotonically increases with current density, mostly owing to the higher rate of production and cell temperature. The flow of exergy for vapor and liquid water are also shown in Fig. 8.

Fig. 9 shows the exergy balance of the cell, as described in Eq. (43), for two different methanol solutions in the anode tank. At open circuit voltage of the cell ($I = 0\,\mathrm{A\,m^{-2}}$), there is some exergy flow in due to the liquid water and methanol crossovers through the membrane and, also, methanol evaporation from the anode. However, the entire migrated methanol through the membrane is chemically reacted with water and oxygen at the CCL without producing any useful power. Heat exergy loss to the environment is directly related to the cell temperature and, as seen, increases as the cell current goes up. Though its value is relatively small compared to the exergy flow in and overall exergy loss, the heat exergy loss to the environment is considerable in comparison with the network exergy.

The cell performance is degraded due to exergy destruction—a measure of the magnitudes of the irreversibilities present during operation. There are multiple sources of irreversibilities that exist during the normal operation of a DMFC, including; phase change of condensable species, friction, mixing of multiple components, electric resistance, and the electrochemical reaction. The total exergy loss for a DMFC during operation versus current density for three different methanol concentrations in the tank is shown in Fig. 9. However, more detailed information about the lost exergy and the contribution by each of the sources are provided in Fig. 10, where the term "Other" refers to the exergy loss due to the phase change, mixing of the components in the system, and friction. Exergy loss due to the electrical resistance in the membrane and the contact resistance is relatively small, and defined as follows:

$$\dot{E}x_{\mathrm{lost,res.}} = {I_{\mathrm{H^+}}}^2 \left(R_{\mathrm{contact}} + \frac{\delta_{\mathrm{m}}}{\sigma_{\mathrm{m}}} \right) \tag{52}$$

Half reactions at the anode and cathode are in equilibrium conditions when no external overpotential voltage exists. This condition results in a zero net flux of reactants and products in the reaction of interest. However, during the normal operation of a DMFC, external overpotentials are required at both the anode and cathode to force the half reactions to proceed in a desired direction at an acceptable rate. These cause the electrochemical irreversibilities inside the cell, either at the anode or the cathode, and are defined as follows:

$$\begin{aligned} Ex_{\mathrm{lost,a,elec.chem.}} &= I_{\mathrm{H^+}} \cdot \eta_{\mathrm{a}} \\ Ex_{\mathrm{lost,c,elec.chem.}} &= I_{\mathrm{H^+}} \cdot \eta_{\mathrm{c}} \end{aligned} \tag{53}$$

The values of the anode and cathode overpotential exergy losses are directly related to the corresponding transfer coefficients, α_{red} and α_{ox}, which are calibrated by the experimental data of [23]. As shown in Fig. 10, the exergy losses due to the anode and cathode overpotentials are very significant at higher cell current densities.

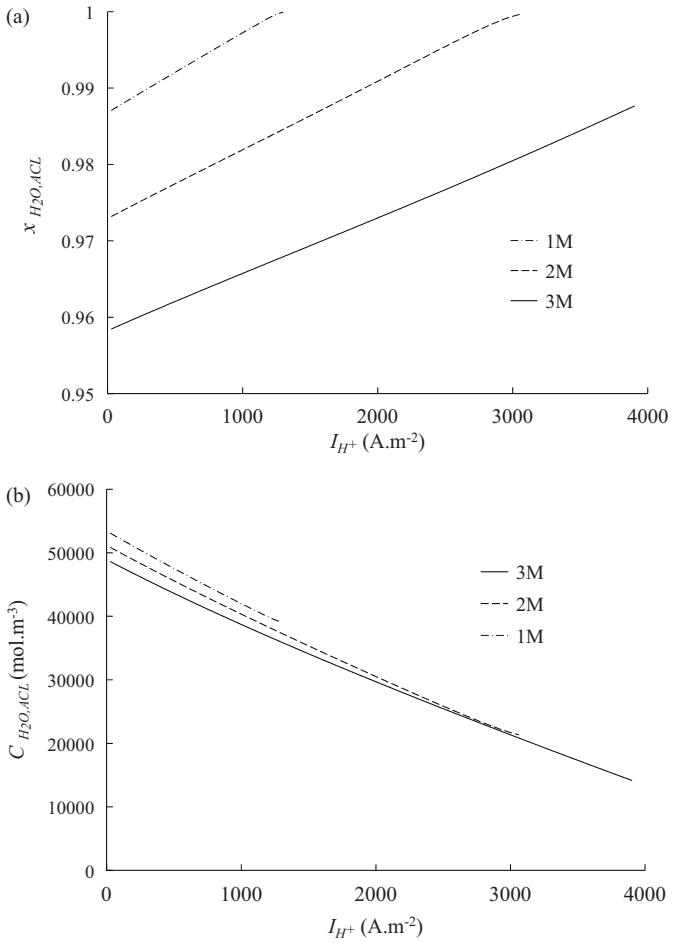

Fig. 6. Variation of (a) molar fraction of water at the ACL, and (b) liquid water concentration at the ACL, versus cell current density.

However, variation of exergy loss contributed by the methanol crossover is different than that by the overpotentials. While the methanol crossover exergy loss monotonically decreases as the cell current density increases for the case of 1 M methanol concentrations at the tank, an initial increase followed by a final reduction is observed when 3 M methanol concentration is fed at the anode.

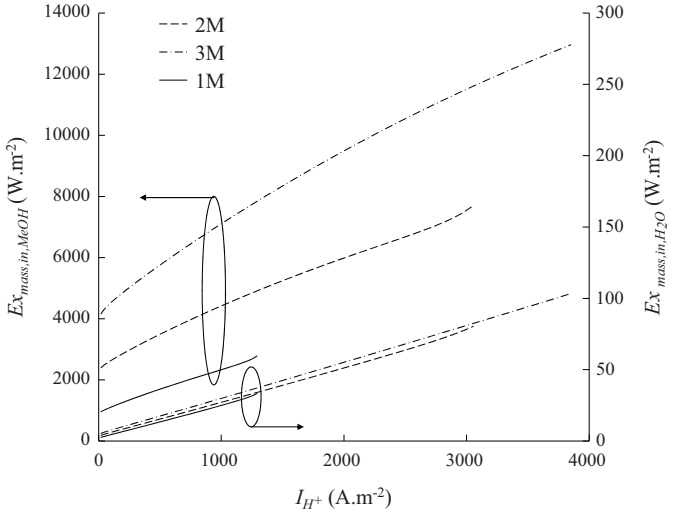

Fig. 7. Exergy flow of liquid water and methanol into the system.

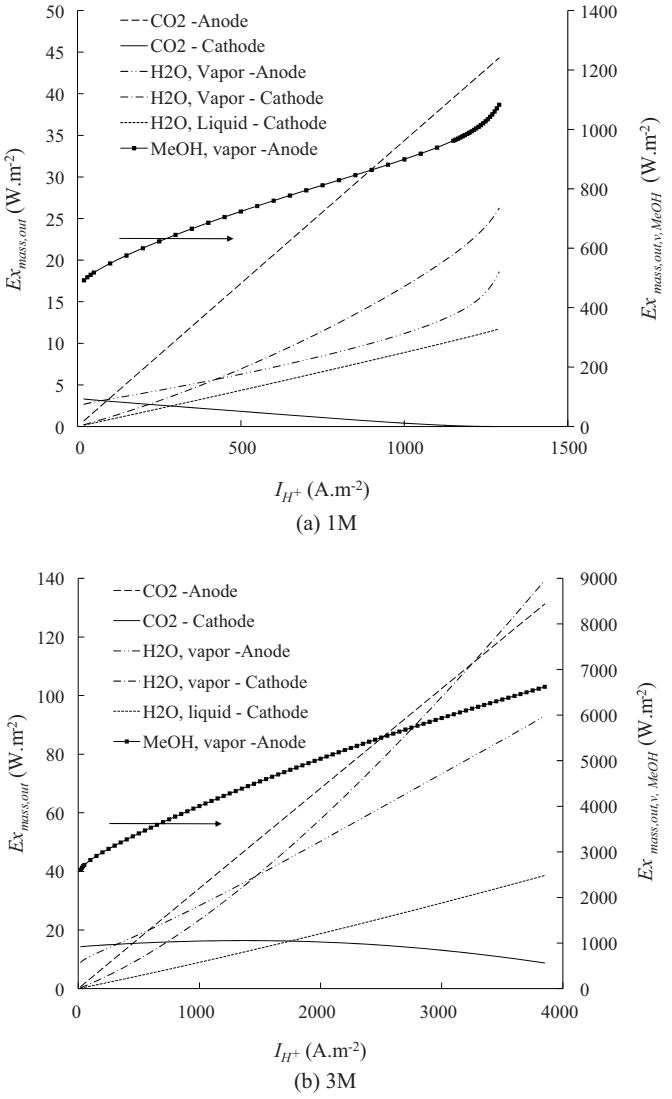

Fig. 8. Exergy flow out of the system by six different components versus cell current densities, when the methanol concentrations in the tank are (a) 1 M, and (b) 3 M.

One of the objectives of the present study is to use the energy and exergy concepts to assess the effectiveness of the DMFC during normal operation. To this end, the first-law and second-law efficiencies are introduced. The first-law efficiency of any conversion device is, by definition, the ratio between useful energy outputs to the total energy inputs. In the case of a DMFC, the maximum first-law efficiency is obtainable when all Gibbs free energy can be converted to electrical energy, and is defined as:

$$\eta_{I,\max} = \frac{\Delta G}{\Delta H} \tag{54}$$

where the lower heating value of fuel is used throughout this study. The maximum first-law efficiency, $\eta_{I,\max}$, is independent of the current density and takes the values of 0.967 and 0.973 when liquid and vapor methanol is respectively supplied at the anode as fuel. However, the real first-law efficiency is much lower than these values and is defined as the ratio of useful work to the energy input:

$$\eta_I = \frac{W_{\text{useful}}}{(\Delta H) \times (I/6F)} \tag{55}$$

Though the first-law efficiency gives some insight about the effectiveness of a DMFC, it cannot assess the effectiveness of energy resource utilization. To this end, the work-second-law efficiency is

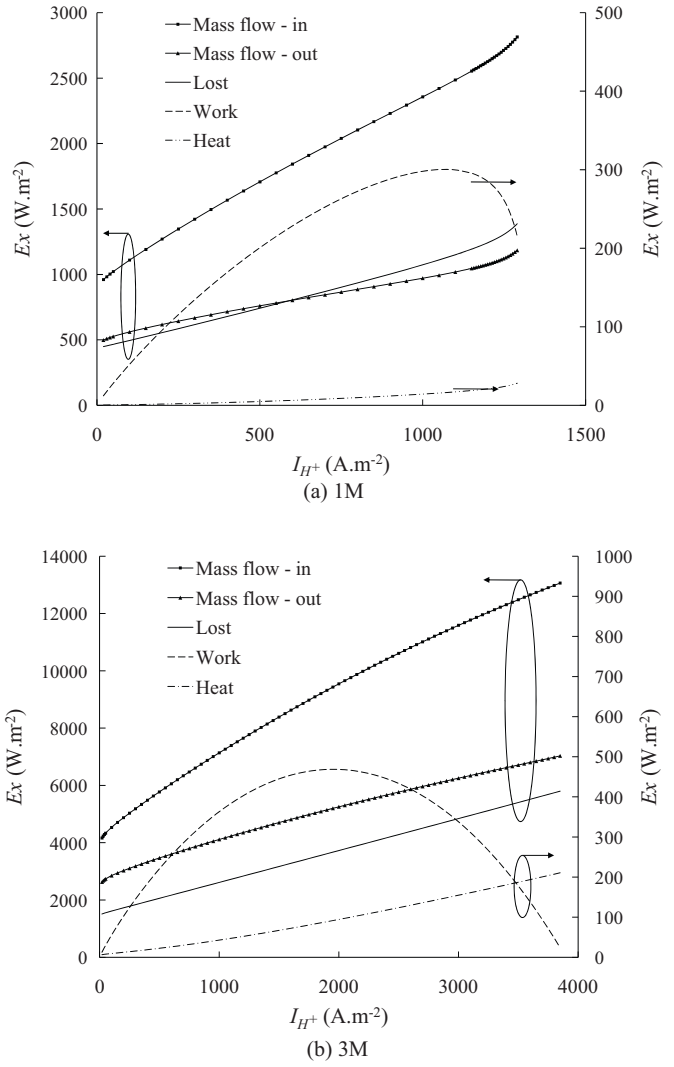

Fig. 9. Exergy balance for the cell at different cell current densities when the methanol concentrations in the fuel tank are (a) 1 M, and (b) 3 M.

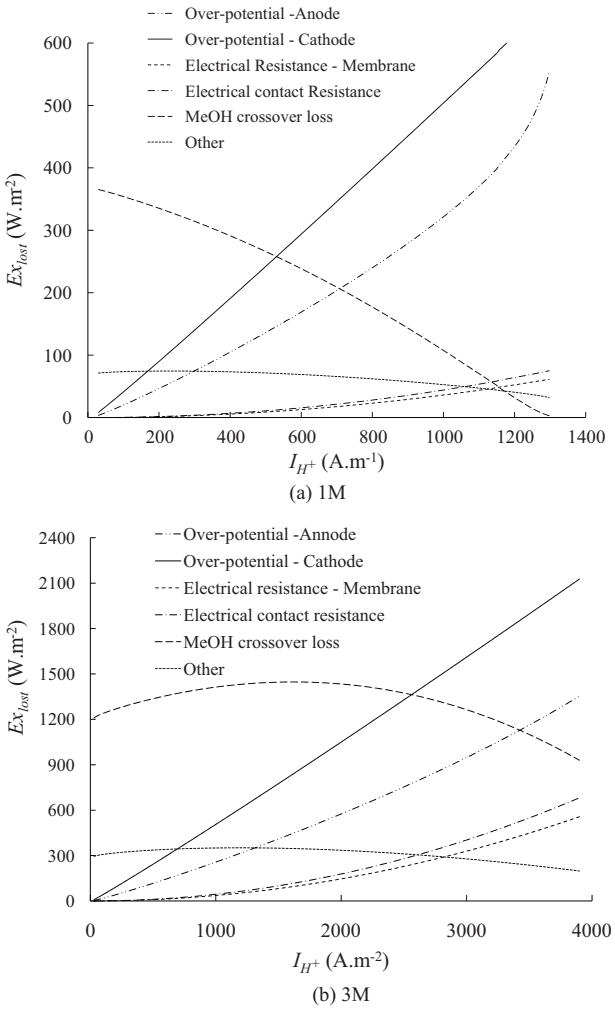

Fig. 10. Different types of irreversibilities present in a DMFC versus cell current when the methanol concentrations in the fuel tank are (a) 1 M, and (b) 3 M.

introduced as follows:

$$\eta_{\mathrm{II,work}} = \frac{\dot{E}x_{\mathrm{work}}}{\sum \dot{E}x_{\mathrm{mass,in}} - \sum \dot{E}x_{\mathrm{mass,out}}} \tag{56}$$

In the same fashion, the heat-second-law efficiency – a measure of assessing exergy loss by heat transfer from the cell to the environment – is defined as:

$$\eta_{\mathrm{II,Heat}} = \frac{\dot{E}x_{\mathrm{Heat}}}{\sum \dot{E}x_{\mathrm{mass,in}} - \sum \dot{E}x_{\mathrm{mass,out}}} \tag{57}$$

Shown in Fig. 11 are the first- and second-law efficiencies versus cell current density for three different methanol concentrations in the anode fuel reservoir. While an increase in the first-law efficiency is observed for higher methanol solution concentrations, the work-second-law efficiency increases as the methanol concentration in the tank decreases. It should be pointed out that the first-law efficiency does not show any optimum condition for the operation of a DMFC, while according to the work-second-law efficiency, there is always an optimum condition for the cell at a specific current density. These optimum current densities are 1210, 1030, and 810 A m^{-2} for 3, 2, and 1 M methanol solutions, respectively, where the corresponding second-law efficiencies are 0.122, 0.162, and 0.224. The lower work-second-law efficiency corresponding to a higher methanol solution is attributed to the higher irreversibilities associated with the methanol crossover (Fig. 10). Another conclusive point in Fig. 11 is the relatively small heat-second-law efficiency ($\eta_{\mathrm{II,Heat}}$) compared to the work-second-law efficiency ($\eta_{\mathrm{II,work}}$), mainly due to the passive operation of the cell in which the

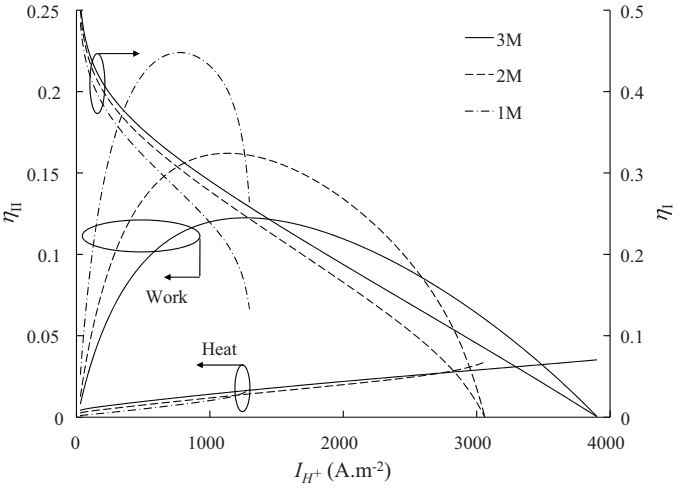

Fig. 11. First- and second-law efficiencies of a passive DMFC versus cell current density for three methanol concentrations in the tank.

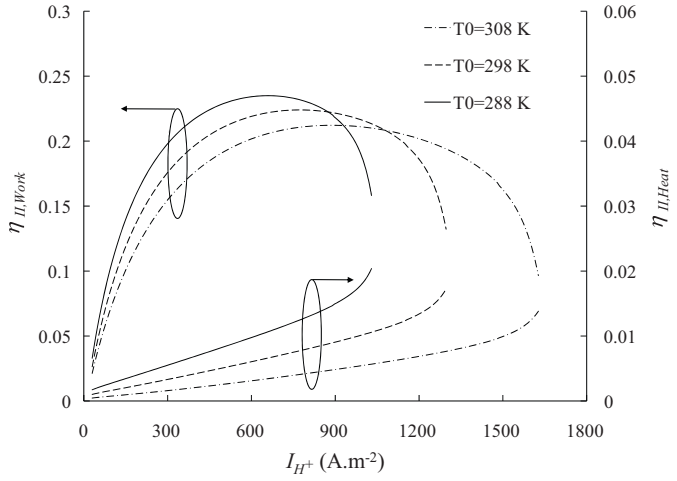

Fig. 12. The effect of ambient temperature on the second-law efficiencies when 1 M methanol solution is fed in the fuel tank.

cell temperature is driven by the internal electrochemical reactions rather than an external heat source.

The assessment of an energy conversion system using the second-law analysis is highly dependent on the definition of the exergy reference environment (dead state). Depicted in Fig. 12 is the effect of the exergy reference ambient temperature on the work- and heat-second-law efficiencies when 1 M methanol concentration is fed at the anode fuel reservoir. As seen in this figure, the colder reference ambient temperature results in better second-law efficiency.

4. Conclusions

The exergy analysis of a passive DMFC provides more detailed information about different types of irreversibilities present inside the cell. The following conclusions are made upon reviewing the above results:

- Methanol crossover in conjunction with the anode and cathode overpotentials contributes the largest portion of the irreversibilities inside the cell. While the methanol crossover contribution is mostly significant for lower current densities, the exergy loss due to overpotentials are more important at higher current densities.
- The work-second-law efficiency of a passive DMFC is monotonically decreases as the methanol solution becomes more concentrated. In other words, a lower concentration of methanol in the tank always offers a better work-second-law efficiency.
- Since the cell temperature of a passive DMFC is only affected by the electrochemical reactions at the catalyst layers rather than an external heat source, the heat-second-law efficiency of the cell is low compared to the work-second-law efficiency.
- Cell operating at lower ambient temperature offers a better second-law efficiency.

Acknowledgment

This research was funded by the National Science Foundation (NSF) under agreement No. CBET-0730349.

Appendix A. Overpotentials at the cathode catalyst layer

Both protonic and electronic current densities can be used to derive the overpotentials at the anode and cathode. However, it is more convenient to use the protonic current density, since the electron conductivity of the carbon phase is chosen to be infinity.

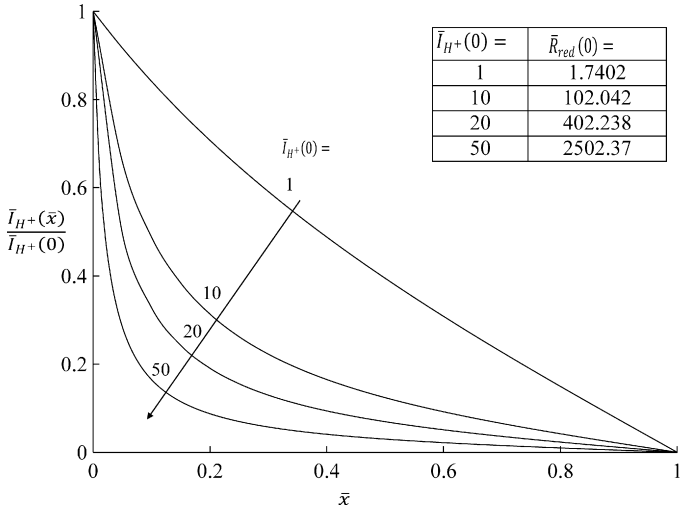

$\bar{I}_{H^+}(0)$ =	$\bar{R}_{red}(0)$ =
1	1.7402
10	102.042
20	402.238
50	2502.37

Fig. A1. Proton current density distribution in the CCL for different cell current density.

Fig. 1(b) displays the solution domain and the coordinate system of solving the cathode overpotential. Upon combining Eqs. (3), (4) and (5) and using the non-dimensional parameters of Eq. (A-1), one arrives at Eq. (A-2):

$$\bar{x} = \frac{x}{L_{CCL}}, \bar{I} = \frac{I}{(2\sigma_m R_u T/\alpha_c F)} = \frac{I}{I^*}, \bar{\eta} = \frac{\eta}{(R_u T/\alpha_c F)} = \frac{\eta}{\eta^*},$$
$$\bar{R}_{red} = \frac{R_{red} \cdot L_{CCL}}{I^*} \quad \text{(A-1)}$$

$$\frac{\partial^2 \bar{I}_{H^+}}{\partial \bar{x}^2} + \frac{\partial (\bar{I}_{H^+})^2}{\partial \bar{x}} = 0 \quad \text{(A-2)}$$

Rewriting Eq. (A-2), the following is concluded:

$$\frac{\partial \bar{I}_{H^+}}{\partial \bar{x}} + \bar{I}^2_{H^+}(\bar{x}) = -\bar{R}_{red}(\bar{x}) + \bar{I}^2_{H^+}(\bar{x}) = -\bar{R}_{red}(0) + \bar{I}^2_{H^+}(0) \quad \text{(A-3)}$$

where $\bar{I}_{H^+}(0)$ denotes the current density at $\bar{x} = 0$, which is identical with the measured current at the external circuit. Also, other non-dimensional parameters are:

$$\begin{cases} \bar{R}_{red}(\bar{x}) = \bar{R}_{0,c} \cdot \exp(\bar{\eta}_c(\bar{x})) \\ \bar{R}_{o,c} = \dfrac{L_{CCL} \cdot (1-s) \cdot a_{red} I^{ref}_{0,O_2}}{I^*} (C_{O_2}/C^{ref}_{O_2})^{\gamma_c} \end{cases} \quad \text{(A-4)}$$

The right hand side of Eq. (A-3) has to be negative [13]. Considering that the CGDL is impermeable to the proton current density, the solution of Eq. (A-3) is

$$\bar{I}_{H^+}(\bar{x}) = \sqrt{\bar{R}_{red}(0) - \bar{I}^2_{H^+}(0)} \tan\left(\sqrt{\bar{R}_{red}(0) - \bar{I}^2_{H^+}(0)}(1-\bar{x})\right) \quad \text{(A-5)}$$

Eq. (A-5) shows an implicit relation between $\bar{I}_{H^+}(0)$ and $\bar{R}_{red}(0)$. For a specific $\bar{I}_{H^+}(0)$, infinite solutions for $\bar{R}_{red}(0)$ exist. However, since there is just one realistic solution for the overpotential, and $\bar{R}_{red}(0)$ has to be finite, the smallest $\bar{R}_{red}(0)$ is the physical solution. Fig. A1 shows the protonic current distribution at the CCL for different cell current densities. As seen, an increase in the cell current density results in a more nonlinear distribution of current density at the CCL. A linear distribution assumption of current density is valid only for low current densities.

Unfortunately, an explicit relation between $\bar{I}_{H^+}(0)$ and $\bar{R}_{red}(0)$ cannot be obtained. However, Kulikovsky [25] solved Eq. (A-5), at $\bar{x} = 0$, for small and large values of $\bar{I}_{H^+}(0)$ using the following

approximation

$$\lambda \cdot \tan(\lambda) = \begin{cases} \lambda^2 & \lambda \ll 1 \\ \lambda & \lambda \gg 1 \end{cases} \tag{A-6}$$

An explicit expression for cell current density in terms of non-dimensional cathode overpotential is obtained for two extreme cases, as follows:

$$\bar{I}_{H^+}(0) = \begin{cases} \bar{R}_{0,c} \cdot \exp(\bar{\eta}_c(0)) & \bar{I}_{H^+}(0) \ll 1 \\ \sqrt{\bar{R}_{0,c}} \cdot \exp\left(\dfrac{\bar{\eta}_c(0)}{2}\right) & \bar{I}_{H^+}(0) \gg 1 \end{cases} \tag{A-7}$$

Now, overpotential can easily be written in term of current density of the cell.

$$\bar{\eta}_c(0) = \begin{cases} \ln(\bar{I}_{H^+}(0)) - \ln(\bar{R}_{0,c}) & \bar{I}_{H^+}(0) \ll 1 \\ 2 \cdot \ln(\bar{I}_{H^+}(0)) - \ln(\bar{R}_{0,c}) & \bar{I}_{H^+}(0) \gg 1 \end{cases} \tag{A-8}$$

Looking at Eq. (A-8), one concludes that the only difference between the overpotentials at two extreme non-dimensional current densities is the first term at the right hand side of Eq. (A-8). In order to have the above relation for the entire range of non-dimensional current density, a fitting function is used as the following [25]:

$$\bar{\eta}_c(0) = \psi(\bar{I}_{H^+}(0)) \cdot \ln(\bar{I}_{H^+}(0)) - \ln(\bar{R}_{0,c}) \tag{A-12}$$

where

$$\psi(\bar{I}_{H^+}(0)) = 1 + \frac{1}{1 + \bar{I}_{H^+}(0)} \tag{A-13}$$

The same procedure is taken for the anode overpotential. It should be pointed out that all the non-dimensional parameters have to be redefined based on the anode parametric values. Also, note that in the text for the sake of convenience, $\bar{I}_{H^+}$ is used in replace of $\bar{I}_{H^+}(0)$.

References

[1] M.J. Moran, H.N. Shapiro, Fundamentals of Engineering Thermodynamics, 6th ed., John Wiley&Sons Inc., New Jersey, 2008.
[2] S.R. Narayanan, T.I. Valdez, N. Rohatgi, in: W. Vielstich, A. Lamm, H.A. Gasteiger (Eds.), Handbook of Fuel Cells, Fundamentals, Technology and Application, vol. 3, John Wiley & Sons Ltd., Chichester, 2003, p. 894.
[3] H.A. Arico, S. Srinivasan, V. Antonucci, Fuel Cells 1 (2001) 133–134.
[4] C.L. Haynes, W.J. Wepfer, ASME J. Energy Resour. Technol. 124 (2002) 95–104.
[5] S.P. Harvey, H.J. Richter, ASME J. Energy Resour. Technol. 116 (1994) 312–318.
[6] K.W. Bedringas, I.S. Erstesvag, S. Byggstoyl, B.F. Magnussen, Energy 22 (4) (1997) 403–412.
[7] S.H. Chan, C.F. Low, O.L. Ding, J. Power Sources 103 (2002) 188–200.
[8] A. Kazim, Energy Convers. Manage. 45 (11–12) (2004) 1949–1961.
[9] M.M. Hussain, J.J. Baschuk, X. Li, I. Dincer, Int. J. Therm. Sci. 44 (9) (2005) 903–911.
[10] M. Ay, A. Midilli, I. Dince, Int. J. Energy Res. 30 (2006) 307–321.
[11] A. Ishihara, Sh. Mitsushima, N. Kamiya, K. Ota, J. Power Sources 126 (1–2) (2004) 34–40.
[12] X. Li, Y. He, B. Yin, Z. Miao, X. Li, J. Power Sources 178 (1) (2008) 344–352.
[13] A. Kulikovsky, Electrochem. Commun. 4 (4) (2002) 318–323.
[14] H. Bahrami, A. Faghri, J. Fuel Cell Sci. Technol. 7 (2010) 015006FCT.
[15] K. Scott, P. Argyropoulos, K. Sundmacher, J. Electroanal. Chem. 477 (2) (1999) 97–110.
[16] H. Bahrami, A. Faghri, Int. J. Heat Mass Transfer 53 (2010) 2563–2578.
[17] B. Xiao, H. Bahrami, A. Faghri, J. Power Sources 195 (2010) 2248–2259.
[18] M. Graetzel, P. Infelta, The Bases of Chemical Thermodynamics, vol. 2, Universal Publishers, 2000, p. 375.
[19] Z. Jiang, J. Zhang, L. Dong, J. Zhuang, J. Electroanal. Chem. 469 (1999) 1–10.
[20] M.J. Lampinen, M. Fomino, J. Electrochem. Soc. 140 (1993) 3537–3546.
[21] A. Faghri, Y. Zhang, Transport Phenomena in Multiphase Systems, Academic Press-Elsevier, Inc., Burlington, MA, 2006.
[22] K.S. Udell, Int. J. Heat Mass Transfer 28 (2) (1985) 485–495.
[23] C. Xu, A. Faghri, X. Li, T. Ward, Int. J. Hydrogen Energy 35 (4) (2010) 1769–1777.
[24] J.P. Meyers, J. Newman, J. Electrochem. Soc. 149 (6) (2002) A729–A735.
[25] A. Kulikovsky, Electrochem. Commun. 4 (12) (2002) 939–946.
[26] H. Bahrami, A. Faghri, J. Electrochem. Soc. 157 (12) (2010) 0013–4651.
[27] C. Xu, T.S. Zhao, W.W. Yang, J. Power Sources 178 (2008) 291–308.
[28] J. Rice, A. Faghri, J. Heat Transfer 130 (6) (2008).
[29] C.L. Yaws, Handbook of Thermodynamic and Physical Property Data, Gulf, Houston, TX, 1992.